REPORT

6PPD-quinone affects the photosynthetic carbon fixation in cyanobacteria by extracting photosynthetic electrons

Xiuqi You,[1,2] Ximin Chen,[1,2] Yi Jiang,[3] Huan Chen,[4] Juan Liu,[1,2] Zhen Wu,[1,2] Weiling Sun,[1,2,*] and Jinren Ni[1,2]

*Correspondence: wlsun@pku.edu.cn

GRAPHICAL ABSTRACT
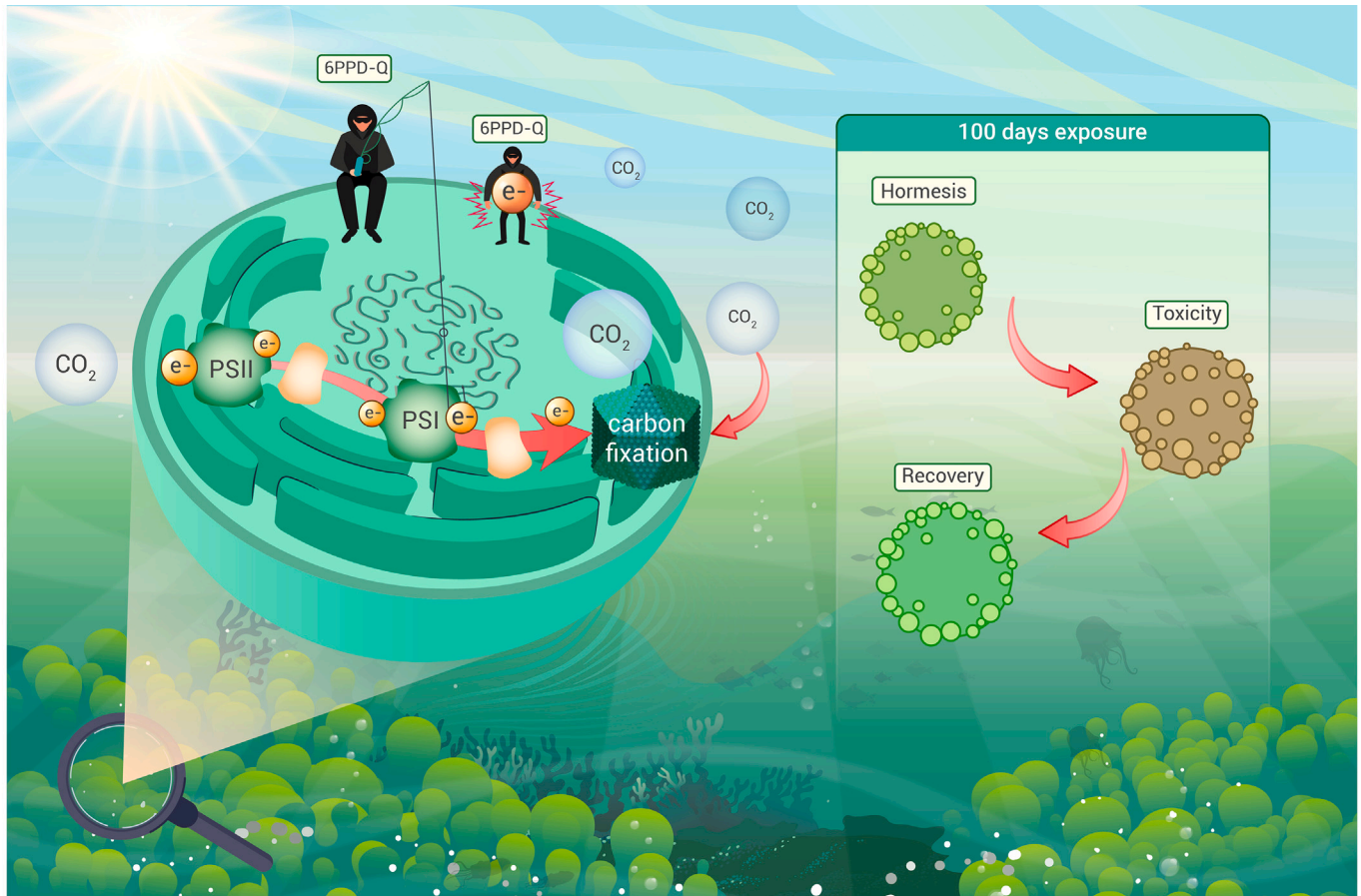
PUBLIC SUMMARY

- *Synechocystis* sp. undergoes hormesis, toxicity, and recovery over 400 generations of exposure to 6PPD-Q.

- 6PPD-Q accepts electrons from the photosynthetic electron transport chain of *Synechocystis* sp.

- 6PPD-Q may impact the carbon cycle by interfering with the photosynthetic electron transport of cyanobacteria.

6PPD-quinone affects the photosynthetic carbon fixation in cyanobacteria by extracting photosynthetic electrons

Xiuqi You,[1,2] Ximin Chen,[1,2] Yi Jiang,[3] Huan Chen,[4] Juan Liu,[1,2] Zhen Wu,[1,2] Weiling Sun,[1,2,*] and Jinren Ni[1,2]

[1]Key Laboratory of Water and Sediment Sciences, Ministry of Education, College of Environmental Sciences and Engineering, Peking University, Beijing 100871, China
[2]State Environmental Protection Key Laboratory of All Material Fluxes in River Ecosystems, Beijing 100871, China
[3]Department of Civil and Environmental Engineering, The Hong Kong Polytechnic University, Hung Hom, Kowloon, Hong Kong 999077, China
[4]Department of Environmental Engineering and Earth Sciences, Clemson University, Clemson, SC 29634, USA
*Correspondence: wlsun@pku.edu.cn

Photosynthetic carbon fixation by cyanobacteria plays a pivotal role in the global carbon cycle but is threatened by environmental pollutants. To date, the impact of quinones, with electron shuttling properties, on cyanobacterial photosynthesis is unknown. Here, we present the first study investigating the effects of an emerging quinone pollutant, i.e., 6PPD-Q (N-(1,3-dimethylbutyl)-N′-phenyl-p-phenylenediamine-quinone), on the cyanobacterium *Synechocystis* sp. over a 400-generation exposure period. *Synechocystis* sp. exhibited distinct sequential phases, including hormesis, toxicity, and eventual recovery, throughout this exposure. Extensive evidence, including results of thylakoid membrane morphological and photosynthetic responses, carbon fixation rate, and key gene/protein analyses, strongly indicates that 6PPD-Q is a potent disruptor of photosynthesis. 6PPD-Q accepts photosynthetic electrons at the plastoquinone Q_B site in photosystem II (PSII) and the phylloquinone A_1 site in PSI, leading to a sustained decrease in the carbon fixation of cyanobacteria after an ephemeral increase. This work revealed the specific mechanism by which 6PPD-Q interferes with photosynthetic carbon fixation in cyanobacteria, which is highly important for the global carbon cycle.

INTRODUCTION

Photosynthesis is vital for Earth's primary productivity.[1,2] Cyanobacteria, as primitive and widely distributed phototrophic organisms in both freshwater and ocean environments, contribute to 20%−30% of the global primary production on earth.[3−5] These organisms regulate biogeochemical cycles and influence the dynamics of aquatic food chains.[3−5] Environmental factors, such as pH, nutrients, and light, affect the photosynthetic efficiency of cyanobacteria.[6] Additionally, widespread chemical pollution poses a significant threat to global aquatic ecosystems.[7,8] Although acute and high-dose exposure to pollutants causes growth inhibition, changes in cellular constituents, and photosynthetic damage in cyanobacteria,[9−11] long-term effects of pollutants at environmentally relevant concentrations on primary production have received limited attention. Consequently, the impact of pollutants in natural aquatic environments on the global carbon cycle remains largely unrecognized.[9]

Quinones, which are both endogenous and xenobiotic compounds, are commonly found in natural environments.[12] However, their ecotoxicity toward aquatic primary producers has received less attention than that of other pollutants, such as antibiotics,[13] nanomaterials,[14] and microplastics.[15] Xenobiotic quinones, known for their high redox activity, have the potential to interfere with biochemical redox reactions involving endogenous quinones.[16,17] In the photosynthetic electron transport process, plastoquinones (Q_A and Q_B) in the photosystem II (PSII) complex and phylloquinones (A_{1A} and A_{1B}) in the PSI complex[18] serve as crucial electron and proton carriers.[17,18] However, exogenous quinones can participate in this quinone redox process. Moreover, synthetic benzoquinone derivatives, known for their oxidant and electrophilic properties, have been identified as exogenous electron acceptors in photosynthesis.[19,20] These xenobiotic quinones are therefore exploited in biophotovoltaics to enhance photocurrent generation by extracting charge from microalgal/cyanobacterial photosystems.[19,20] This raises concerns regarding the potential disruption of photosynthesis by xenobiotic quinones in aquatic environments. The detrimental effects of quinones on cyanobacteria are still a substantial knowledge gap in the assessment of the ecotoxicity risk of quinone pollutants.

A highly toxic quinone, 6PPD-quinone (6PPD-Q; N-(1,3-dimethylbutyl)-N′-phenyl-p-phenylenediamine-quinone), has been identified as the primary culprit responsible for urban runoff mortality syndrome in coho salmon.[21] This compound is a quinone derivative of the tire antioxidant 6PPD, which is released into the aquatic environment through the leaching of particles from tires onto pavement and subsequent surface runoff.[21] Given the extensive application of its precursor compound 6PPD,[22] 6PPD-Q is inferred to be a globally distributed pollutant, with concentrations ranging from 0.8 to 19 μg/L in roadway runoff,[21] 80−370 ng/L in snowmelt,[23] and 0.38−2.30 μg/L in surface water.[24−26] To date, the toxicological effects of 6PPD-Q have gained intensive attention worldwide.[21,27,28] Nevertheless, the impact of 6PPD-Q on aquatic primary producers and its subsequent ecological implications are poorly understood. Considering the potential of quinones to shuttle electrons, it is plausible to hypothesize that 6PPD-Q can disrupt the photosynthetic process, causing adverse effects on aquatic primary producers.

Here, we investigated the potential of 6PPD-Q to interfere with the photosynthetic carbon fixation process in a model cyanobacterium (*Synechocystis* sp. PCC 6803). We hypothesize that 6PPD-Q may compete with plastoquinones/phylloquinones for electrons in the photosynthetic electron transport chain (ETC). This competition can result in alterations in the flow of photogenerated electrons, ultimately affecting CO_2 reduction in cyanobacteria. To test our hypothesis, we conducted a long-term study (100 days, approximately 400 generations) exposing *Synechocystis* sp. to environmentally relevant concentrations of 6PPD-Q. 6PPD-Q initially triggered a hormetic response in the cyanobacterium during a 16-generation (4-day) exposure. However, this hormetic response converted to toxicity over time and gradually recovered after 240 generations of exposure. Furthermore, we elucidated the specific targets through which 6PPD-Q acts on the photosynthetic ETC and found that 6PPD-Q disrupted the balance between the captured light energy and metabolic energy demand in the cyanobacterium. Ultimately, 6PPD-Q caused a sustained decrease in carbon fixation by *Synechocystis* sp..

RESULTS

Hormone response to 6PPD-Q

For acute exposure (4 days), the cell density of *Synechocystis* sp. presented an inverted U-shaped dose-dependent response to 6PPD-Q ranging from 0.01 to 100 μg/L (Figure 1A), indicating the hormetic response of *Synechocystis* sp. to short-term exposure to 6PPD-Q. The greatest hormetic stimulation was observed at a dose of 0.1 μg/L 6PPD-Q, resulting in an ∼14% increase in cell density. In contrast, 6PPD-Q exposure inhibited reactive oxygen species (ROS) production and the activities of antioxidant enzymes, including superoxide dismutase (SOD) and catalase (CAT) (Figure 1B). Alongside the stimulated growth, the photosynthetic performance of *Synechocystis* sp. was enhanced by 6PPD-Q, as reflected by the improved photochemical efficiency (Figure 1C). Intriguingly, the hormetic responses observed in *Synechocystis* sp. did not occur under light-activated heterotrophic growth conditions, suggesting that 6PPD-Q caused hormesis specifically through its effects on photosynthesis (Figure S1). These hormetic responses in *Synechocystis* sp. can be attributed to the overcompensation of photosynthesis stimulated by 6PPD-Q.[29−31]

Hormesis is not a "free lunch," and hermetic stimulation cannot occur for all traits under mild stress.[32,33] While 6PPD-Q stimulated cell proliferation and photosynthesis, this promotion came at the expense of other
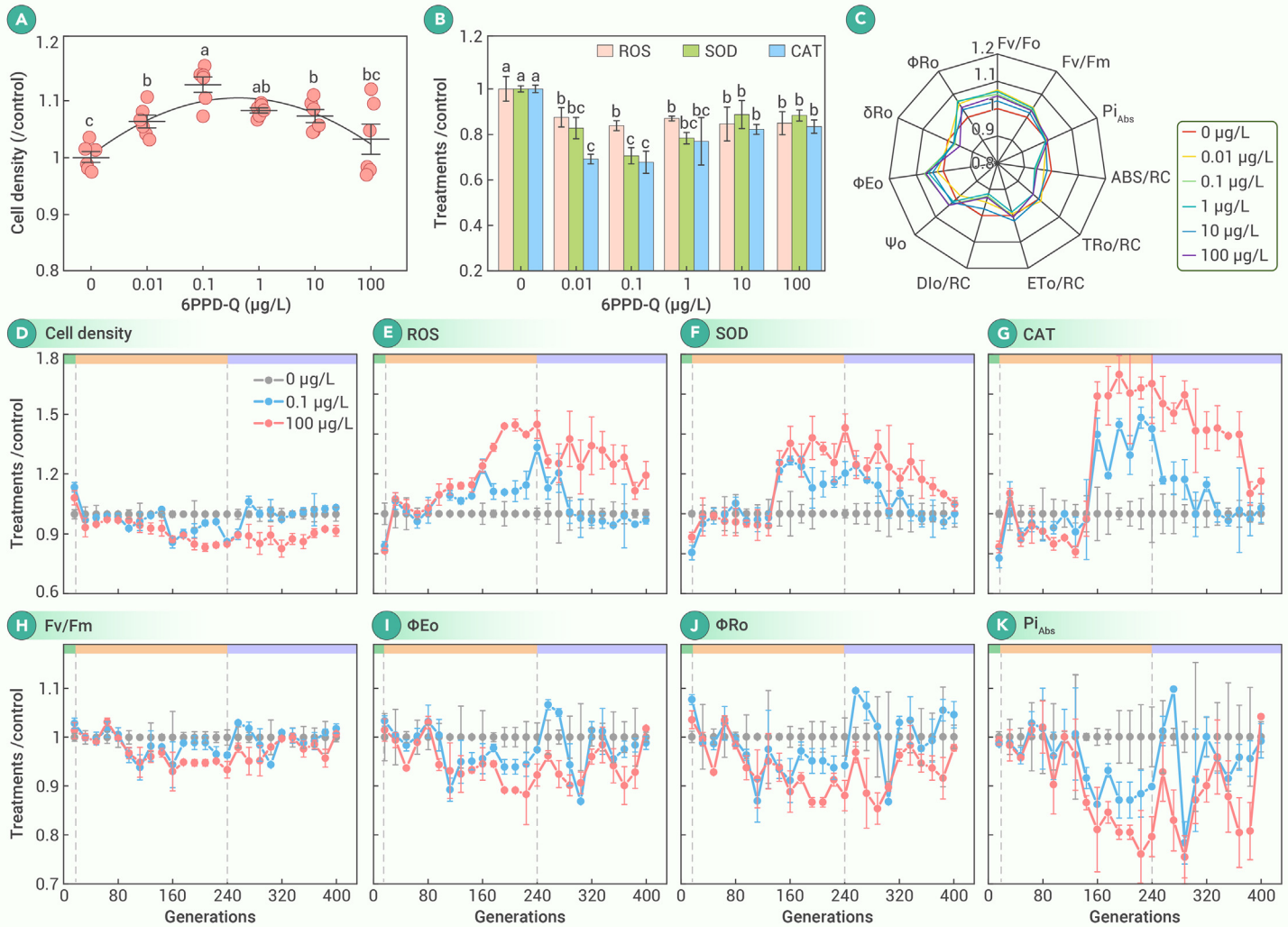
Figure 1. Effects of 6PPD-Q on *Synechocystis* sp. (A−C) Cell density (A); oxidative stress (B), including ROS levels, SOD activity, and CAT activity; and chlorophyll fluorescence parameters (C) of *Synechocystis* sp. exposed to 0−100 µg/L 6PPD-Q for 4 days (significant differences in cell density, ROS levels, SOD activity, and CAT activity among different treatments are marked with different letters, one-way ANOVA). (D−K) Cell growth (D), ROS generation (E), SOD activity (F), CAT activity (G), and photosynthetic performance (H−K) of *Synechocystis* sp. exposed to 6PPD-Q at 0, 0.1, and 100 µg/L across 400 generations.

important traits, such as decreased activity of antioxidant enzymes (Figure 1B) and CO_2-fixing enzymes (Figure S2), which is a known hormetic trade-off.

Three phases of long-term response: Hormesis, toxicity, and recovery

To uncover any potential risks that might be masked by hormetic responses, a comprehensive 400-generation exposure test was carried out. *Synechocystis* sp. exposed to 6PPD-Q for 400 generations underwent three distinct phases: hormesis (G0−G16), toxicity (G16−G240), and recovery (G240−G400) (Figures 1D−1K). During long-term exposure, the hormetic responses of *Synechocystis* sp. to 6PPD-Q were limited to the first 16 generations (G0−G16). Subsequently, the detrimental effects of 6PPD-Q became apparent during G16−G240, followed by a recovery phase (Figures 1D−1K). During the toxicity phase (G16−G80), 6PPD-Q exhibited subtoxic effects on *Synechocystis* sp., resulting in decreases in cell density of approximately 3% and 7% when exposed to 0.1 and 100 µg/L 6PPD-Q, respectively (Figure 1D). However, the toxicity of 6PPD-Q increased during the G80−G240 generations (Figure 1D), leading to significant reductions in cell density of approximately 14% and 15% when the cells were continuously exposed to 0.1 and 100 µg/L 6PPD-Q, respectively, for 240 generations. After G240, *Synechocystis* sp. began to exhibit biological adaptation. The cell density of *Synechocystis* sp. exposed to 0.1 µg/L 6PPD-Q recovered to levels comparable to those of the control at G288 and remained stable during G288−G400 (Figure 1D). Unlike at low concentrations, *Synechocystis* sp. exposed to high concentrations of 6PPD-Q (100 µg/L) failed to recover to the control level within 400 generations (Figure 1D). Overall, *Synechocystis* sp. experienced biomass losses of

approximately 9% and 37% during 100 days of exposure to 0.1 and 100 µg/L 6PPD-Q, respectively.

In response to the hormetic effect, the level of ROS and SOD and CAT activities in *Synechocystis* sp. decreased within G16 (Figures 1E−1G). Afterward, during G16−G80, the ROS levels were comparable to those in the control group but increased notably from G80 to G240 (Figure 1E). Similar trends were observed for the activities of SOD and CAT, with a slight delay during G80−G240 (Figures 1F and 1G), indicating an activated antioxidant response to the stress caused by 6PPD-Q. Moreover, the levels of ROS and SOD and CAT activities were greater in *Synechocystis* sp. exposed to 100 µg/L 6PPD-Q than in those exposed to 0.1 µg/L 6PPD-Q. During the recovery phase of G240−G400, the elevated ROS levels in *Synechocystis* sp. exposed to 0.1 µg/L 6PPD-Q gradually decreased to levels comparable to those of the control by G288, along with a delayed recovery of SOD and CAT activities (Figures 1E−1G). The recovery of *Synechocystis* sp. from exposure to 100 µg/L 6PPD-Q was more challenging than that from 0.1 µg/L 6PPD-Q.

The chlorophyll fluorescence parameters, including the maximum quantum efficiency of PSII (Fv/Fm), the efficiency of electron transport from PSII to PSI (ΦEo), and the quantum yield for the reduction of the end electron acceptors at PSI (ΦRo), were stimulated by 6PPD-Q during the first 16 generations. These parameters then fluctuated at levels similar to those of the control group from G16 to G80 before decreasing significantly between G80 and G240 (Figures 1H−1J). A similar pattern was observed for the performance indices (PI$_{Abs}$) (Figure 1K). This indicates that photosynthetic dysregulations occurred in *Synechocystis* sp. during prolonged exposure to 6PPD-Q. Moreover, the

deterioration of the photosynthetic performance between G80 and G240 was more prominent in *Synechocystis* sp. exposed to 100 μg/L 6PPD-Q than in those exposed to 0.1 μg/L 6PPD-Q. Similarly, the inhibited photosynthetic parameters gradually returned to levels comparable to those of the control during the recovery phase (G240−G400), supporting the recovery of *Synechocystis* sp. during this period. Similarly, the photosynthetic pigments also exhibited similar phasic changes (Figure S3).

Phasic changes in photophysiological performance

To investigate the assumption that 6PPD-Q affects photosynthesis in *Synechocystis* sp., the substructure of thylakoid membranes, where the light-driven reactions of photosynthesis occur, was examined. Cells exposed to 0.1 and 100 μg/L 6PPD-Q for 400 generations showed no apparent cell damage (Figure S4), in agreement with the sublethal toxicity of 6PPD-Q. However, there were significant changes in the distances between thylakoid layers. In the hormesis phase, the interthylakoidal distance increased by approximately 20% (51.8 ± 9.2 nm for the 0.1 μg/L 6PPD-Q treatment group and 52.4 ± 8.5 nm for the 100 μg/L 6PPD-Q treatment group, *n* = 120) compared to that of the control group (43.4 ± 7.8 nm, *n* = 120) (Figure 2A). In the toxicity phase, the distances decreased by approximately 10% (40.5 ± 6.2 nm for the 0.1 μg/L 6PPD-Q treatment group, *n* = 120) compared to those of the control group (43.8 ± 7.9 nm, *n* = 120) (Figure 2B). During the recovery phase, there was no significant difference compared to the control (42.9 ± 8.2 nm, *n* = 120) (Figure 2C). Three-dimensional tomogram reconstruction (Figures 2D−2F) further confirmed these changes. The space between the thylakoid layers should be sufficient for double-row light-harvesting antenna complexes (phycobilisomes [PBSs]).[34,35] Therefore, the enlarged and shrunken spaces between the thylakoid layers in the hormesis and toxicity phases, respectively, indicate the up- and downregulated light-harvesting ability in *Synechocystis* sp. upon 6PPD-Q exposure.

To further evaluate the impact of 6PPD-Q exposure on photosynthetic activity, changes in oxygen exchange were measured. In the hormesis phase (G16), photosynthetic activity was stimulated, while respiration activity was inhibited, leading to an increase in carbon use efficiency (Figures S5A and S5B). In contrast, in the toxicity phase (G240), photosynthetic activity decreased, while respiration activity increased (Figures S5C and S5D), resulting in lower carbon use efficiency and cell density than in the control (Figures S5C and S5D). During the recovery phase (G400), photosynthetic activity increased, and respiratory activity decreased again (Figures S5E and S5F), enabling energy accumulation for self-rescue. These findings provide insights into the dynamic modulation of photosynthetic and respiratory activities in response to 6PPD-Q exposure.

To elucidate the mechanisms by which 6PPD-Q affects photosynthetic processes (Figure 3A), we examined electron generation (PSII and PSI activity), energy transduction (ATP and NADPH levels), and electron terminal consumption for CO_2 fixation (Rubisco and Rubisco activase [RCA] activity) (Figure 3A). In the hormesis phase, PSII activity was significantly enhanced under 0.1 μg/L 6PPD-Q exposure (Figure 3B). However, no significant difference was observed in PSI activity over 400 generations of exposure (Figures 3B−3D). Photochemically generated electrons travel from water through PSII, cytochrome bf (Cyt bf), and PSI to reduce $NADP^+$-coupled generation of NADPH and ATP (Figure 3A).[36-38] The increased PSII activity coincided with a notable increase in NADPH and ATP levels at G16 (Figure 3B). NADPH and ATP serve as chemical energy sources for the Calvin-Benson-Bassham (CBB) cycle, which drives carbon assimilation (Figure 3A). CO_2 is the terminal acceptor of photosynthetic electrons in the CBB cycle,[37] and photosynthetic CO_2 reduction is catalyzed by Rubisco.[39] The activity of Rubisco and RCA, enzymes involved in CO_2 fixation, was severely inhibited in G16 (Figure 3B). Therefore, the enlarged electron source, increased electron flow for NADPH synthesis, and reduced carbon assimilation caused the accumulation of ATP and NADPH during the hormesis phase (Figure 3E). In addition to NADPH, oxygen serves as another electron sink in cyanobacteria and can be reduced by photosynthetic electrons to generate ROS (Figure 3A).[40] An increase in the NADPH sink resulted in reduced electron leakage to molecular oxygen, thereby decreasing ROS generation (Figure 1E).

PSII activity was significantly inhibited during the toxicity phase (G16−G240), and the levels of NADPH and ATP gradually decreased (Figures 3C, S6A, and S6B). Notably, the two electron sinks, ROS (Figure 1E) and NADPH (Figures 3B and 3C), exhibited opposite trends. This suggests that 6PPD-Q redirects electrons toward the oxygen reduction pathway, reducing the availability of electrons

for NADPH synthesis during G16−G240. Moreover, the suppressed activities of Rubisco and RCA gradually recovered from G16 to G160 and were promoted at G240 (Figures 3C, S6C, and S6D). Overall, in cells in the toxicity phase, the photosynthetic electron source was damaged, resulting in increased electron leakage to oxygen for ROS generation. The production of NADPH and ATP decreased, while the activity of the CO_2-fixing enzyme Rubisco increased (Figure 3F). During the recovery phase, the suppressed PSII activity observed during the toxicity phase was alleviated. The ATP and NADPH levels gradually returned to the control levels at G400, and the activities of Rubisco and RCA also recovered (Figures 3D and S6). These results suggest that photosynthetic electron production, the distribution of electron sinks, and the consumption of electrons for CO_2 reduction established a new balance after prolonged exposure to 6PPD-Q (Figure 3G).

Dysfunction of photosynthesis-associated genes and proteins

To gain a comprehensive understanding of the molecular responses induced by 6PPD-Q, transcriptomic and proteomic profiling was performed. Transcriptome-based clustering (Mfuzz) revealed that genes across 400 generations were grouped into ten clusters (Figure S7A). The genes in each cluster were mapped to KEGG pathways (Figure S7A). Clusters 1−3 showed similar trends to those of cell density (Figure 4A), and these clusters were enriched in photosynthesis-related pathways (Figure 4B). Further analysis using gene set enrichment analysis revealed that photosynthesis-related gene sets were significantly enriched during the hormesis phase (G16) (Figure 4C) and gradually downregulated between G80 and G240 (Figures 4D−4F). However, during the recovery phase (G320−G400), the expression of photosynthesis-related genes did not significantly differ between the treatment and control groups (Figures 4G and 4H). Moreover, genes involved in the photosynthetic ETC were activated during the hormesis phase (G16) (Figure 4I) but suppressed during the toxicity phase (G80−G240) (Figures 4J and S8A−S8C). In the recovery phase, the suppressed photosynthetic chain was partly restored (Figures 4K and S8D).

Positive correlations between proteins and genes were observed in samples across the 400 generations (Pearson; $p = 0.027$, $R^2 = 0.001$) (Figure S9). The changes in proteins within clusters 1−3 were consistent with the corresponding gene expression patterns (Figure 4A). Furthermore, long-term changes in photosynthesis, i.e., upregulation, downregulation, and subsequent recovery, were confirmed by both transcriptomic and proteomic analyses (Figure S10). The findings suggest that 6PPD-Q affects the growth of *Synechocystis* sp. by impacting photosynthesis, as shown by the similar trends observed in cell growth and photosynthetic processes. Moreover, among the five components of the photosynthesis pathway (PSII, PSI, Cyt bf, photosynthetic electron transport, and ATPase), the most pronounced variations were observed in PSII and PSI (Figure S10).

Additionally, the changes in genes and proteins involved in light-harvesting PBS (Figure S11) supported the plastic regulation of interthylakoidal distances (Text S1). Central carbon metabolism (Figure 4L) suggested imbalances between energy capture and release, which contributed to the growth fluctuations in *Synechocystis* sp. (Text S2). During the hormesis phase, energy uptake exceeds energy metabolism, resulting in greater cell density (Figure 4L). In contrast, during the toxicity phase, energy metabolism outweighed energy capture (Figures 4L and S12), leading to reduced cell density. Ultimately, in the recovery phase, balanced regulation of energy capture and release enabled the rescue of cells from toxicity (Figures 4L and S12).

6PPD-Q accepted photosynthetic electrons at the Q_B in PSII and at the A_1 in PSI

The photophysiological and omics results provided strong evidence that 6PPD-Q disrupts photosynthesis. To further investigate its mechanism of action, specific targets of 6PPD-Q involved in the photosynthetic process were identified. 6PPD-Q exhibits an appropriate redox midpoint potential (Em) to accept electrons from photosynthetic electron chains because of its more positive Em value (+0.341 V vs. standard hydrogen electrode [SHE]) than that of the typical exogenous electron acceptor 2,6-dichloro-1,4-benzoquinone (Em = +0.315 V vs. SHE) (Figure 5A). According to the biophotovoltaic test (Figure 5B), the addition of 6PPD-Q significantly enhanced photocurrent generation (Figure 5C). This effect was observed only in the presence of *Synechocystis* sp. cells, under illumination, and in the presence of 6PPD-Q, indicating that 6PPD-Q can serve as an electron
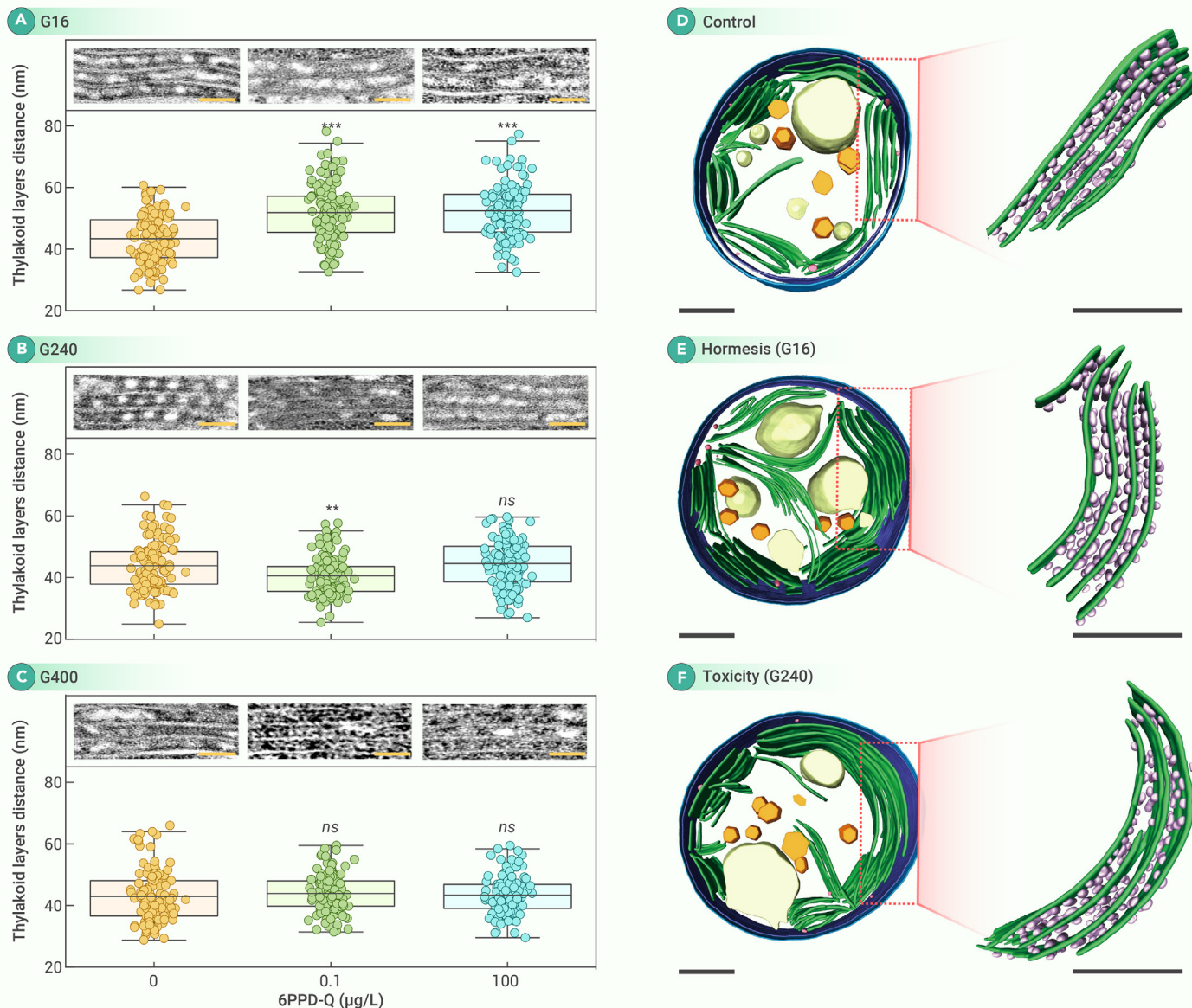
Figure 2. Ultrastructure of thylakoid membranes at the exponential growth phase in *Synechocystis* sp. (A–C) Distance between adjacent thylakoid membrane layers for *Synechocystis* sp. exposed to 6PPD-Q for 16 (G16), 240 (G240), and 400 (G400) generations ($n = 120$ cells from three independent biological replicates for each group). Boxplots show the median value (center line), interquartile range (box), and 1.5 times the interquartile range (whiskers). Representative transmission electron microscopy images are provided above the respective boxes (scale bars, 100 nm). Asterisks indicate significant differences compared to the cells in the control groups, while *ns* represents nonsignificant differences according to one-way ANOVA; significant differences are shown as **$p < 0.01$ and ***$p < 0.001$. (D–F) Morphological transformation of *Synechocystis* sp. exposed to 6PPD-Q at 0.1 µg/L three-dimensional (3D) reconstructions of cells in the control phase, hormetic phase (G16), and toxicity phase (G240) were obtained via focused ion beam scanning electron microscopy; the images show the outer membrane in blue, the plasma membrane in purple, the thylakoid membranes in green, the lipid bodies in red, the carboxysomes in orange, the polyphosphate bodies in yellow, and the phycobilisomes in pink. The parts marked by red boxes with dotted lines were selected to further show the details of the thylakoid membranes. Scale bars, 500 nm. Each 3D segmentation was reconstructed from a 150-nm-thick tomographic section of a unique cell that consisted of single slices with a thickness of 5 nm.

carrier between cells and electrodes by accepting photosynthetic electrons to promote extracellular electron transfer in *Synechocystis* sp..

The electron-accepting sites for 6PPD-Q were unequivocally identified. The presence of 6PPD-Q effectively reversed the inhibition of electron transport caused by 2,5-dibromo-3-methyl-6-isopropylbenzoquinone but not by 3-(3,4-dichlorophenyl)-1,1-dimethylurea (DCMU) (Figure 5D). This suggests that 6PPD-Q can accept photosynthetic electrons at the Q_B site, which is after Q_A and before the Cyt bf complex (Figure 5D). Moreover, 6PPD-Q underwent photo-reduction when electron transport from plastocyanin to the reducing side of PSI was active, while the electrons from PSII were inhibited by DCMU and 2,6-dichlorophen-olindophenol with the addition of ascorbate (DCPIPH$_2$) as an artificial electron donor (Figure 5D). This phenomenon is similar to the electron transfer from DCPIPH$_2$ to methyl viologen (MV) at PSI, where DCPIPH$_2$ acts as the electron donor and MV acts as the electron acceptor (Figure 5D). These results indicate that 6PPD-Q can also accept electrons on the reducing side of PSI. Lotina-Hennsen et al.[18] previously suggested that 2,5-diamino-*p*-benzoquinone deriva-

tives with low water solubility accept electrons at the lipophilic site of PSI, where phylloquinone A_1 is located. Similarly, 6PPD-Q, an exogenous electron mediator with high hydrophobicity (logK_{ow} = 5–5.515),[21] can also harvest electrons at A_1 to F_X in PSI. Docking studies further confirmed that 6PPD-Q can occupy the same binding pocket as plastoquinones and phylloquinones in PSII and PSI, respectively (Figures 5E–5H; Text S3). The docking scores indicated a good fit between 6PPD-Q and these binding pockets, with all docking scores below -7.0 kcal/mol, in the order of $Q_B < A_{1A} < Q_A < A_{1B}$ (Table S2). This suggests that compared with Q_A, 6PPD-Q has a greater propensity to acquire electrons from Q_B and A_1.

Outcome of disturbed photosynthesis: Decrease in carbon fixation

To examine the impact of 6PPD-Q on the photosynthetic electron transfer, we assessed the downstream effects on carbon fixation rates. Initial changes in the ^{13}C assimilation of *Synechocystis* sp. were observed within 18 h of continuous illumination using Raman microscopy (Figures 6A and S13). Subsequently, we
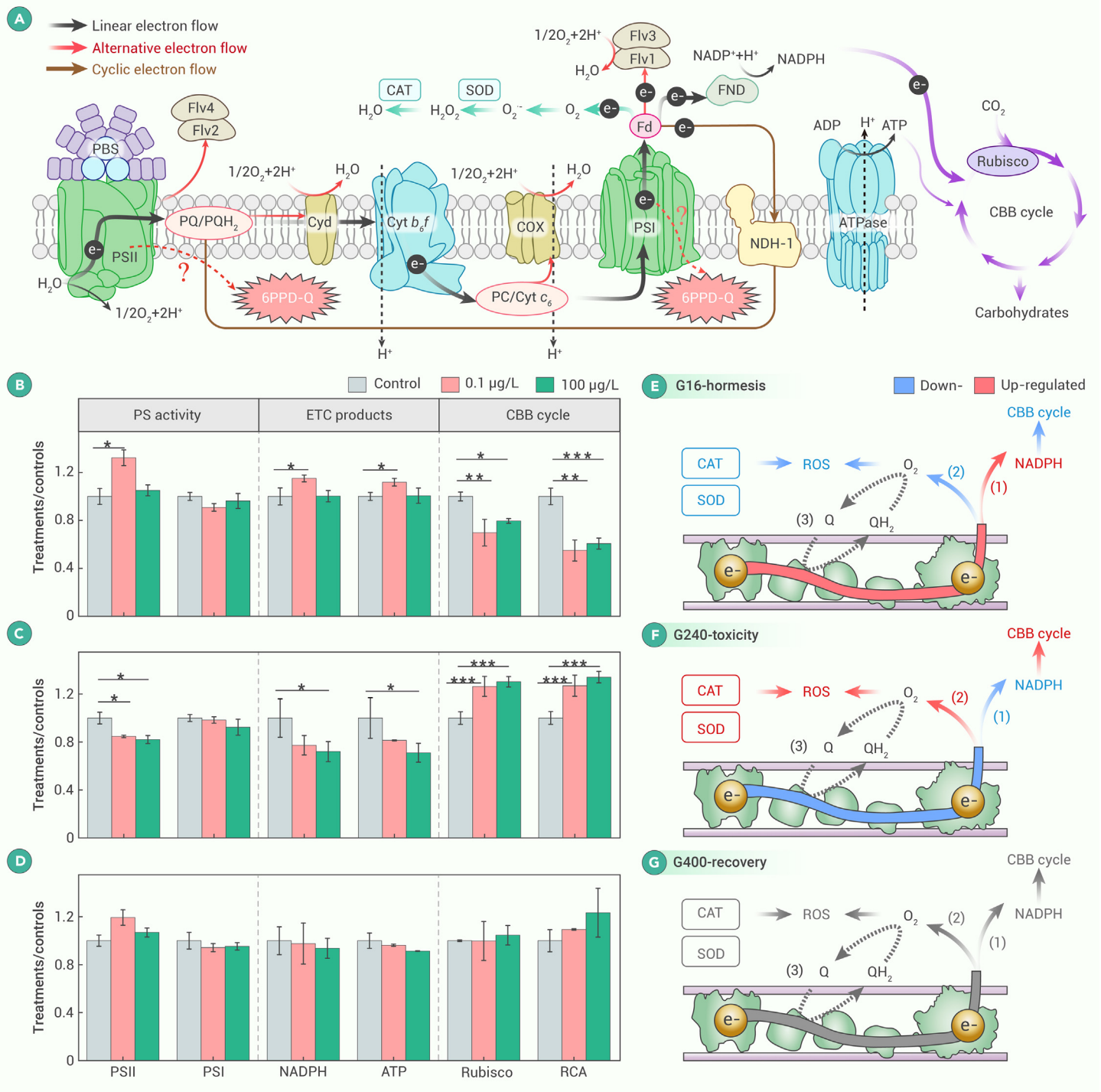
Figure 3. Photosynthesis of *Synechocystis* sp. upon 6PPD-Q exposure (A) Schematic representation of photosynthetic electron transport pathways in *Synechocystis* sp. PCC 6803. Linear electron flow is the dominant path for photosynthetic electron flow, which transports electrons from water to NADP+ and provides reducing equivalents (NADPH) and energy (ATP) for the CBB cycle (the major sink for photosynthetic electrons). When the sink capacity of the CBB cycle is insufficient, alternative electron flows are responsible for dissipating excess electrons to alternative sinks such that flavodiiron proteins (including Flv1–Flv4) and respiratory terminal oxidases (including Cyd and COX) catalyze the reduction of oxygen to water to avoid the generation of damaging ROS. NADH dehydrogenase-like complex 1 (NDH-1) mediates cyclic electron flow around PSI, providing only ATP for the CBB cycle. Excess electrons that cannot be consumed by sinks leak to oxygen and generate superoxide anions ($O_2 \cdot ^-$), which are scavenged by superoxide dismutase (SOD) and catalase (CAT). (B–D) PSII activity, PSI activity, NADPH content, ATP content, Rubisco activity, and Rubisco activase (RCA) activity of *Synechocystis* sp. exposed to 6PPD-Q during (B) hormesis (the 16th generation [G16]), (C) toxicity (G240), and (D) recovery (G400) phases. Asterisks indicate significant differences compared to the cells in the control groups according to one-way ANOVA; significant differences are shown as *$p < 0.05$, **$p < 0.01$, and ***$p < 0.001$. (E–G) The electron transfer between PSII and PSI, distribution of electron sinks for NADPH generation and ROS production, and electron consumption into the CBB cycle at the (E) hormesis, (F) toxicity, and (G) recovery phases. Red and blue lines indicate upregulation and downregulation, respectively, while the gray line represents an insignificant difference between the 6PPD-Q treatment group and the control group.

quantified the carbon fixation rates of *Synechocystis* sp. using an isotope mass spectrometer. During the hormesis phase (G16), exposure to 0.1 μg/L 6PPD-Q resulted in a slight increase of approximately 7% in the carbon fixation rate (Figure 6B). This suggests that the improved activity of PSII and enhanced electron transfer efficiency in the light-dependent reactions compensated for the reduced

Rubisco activity in the CBB cycle. In the toxicity phase (G240), the carbon fixation rate decreased to 72% of that of the control (Figure 6C). In the recovery phase, although the suppression of carbon fixation was alleviated, it remained at approximately 80% of that of the control (Figure 6D). These findings indicate a long-term adverse effect of 0.1 μg/L 6PPD-Q on carbon fixation in *Synechocystis* sp.
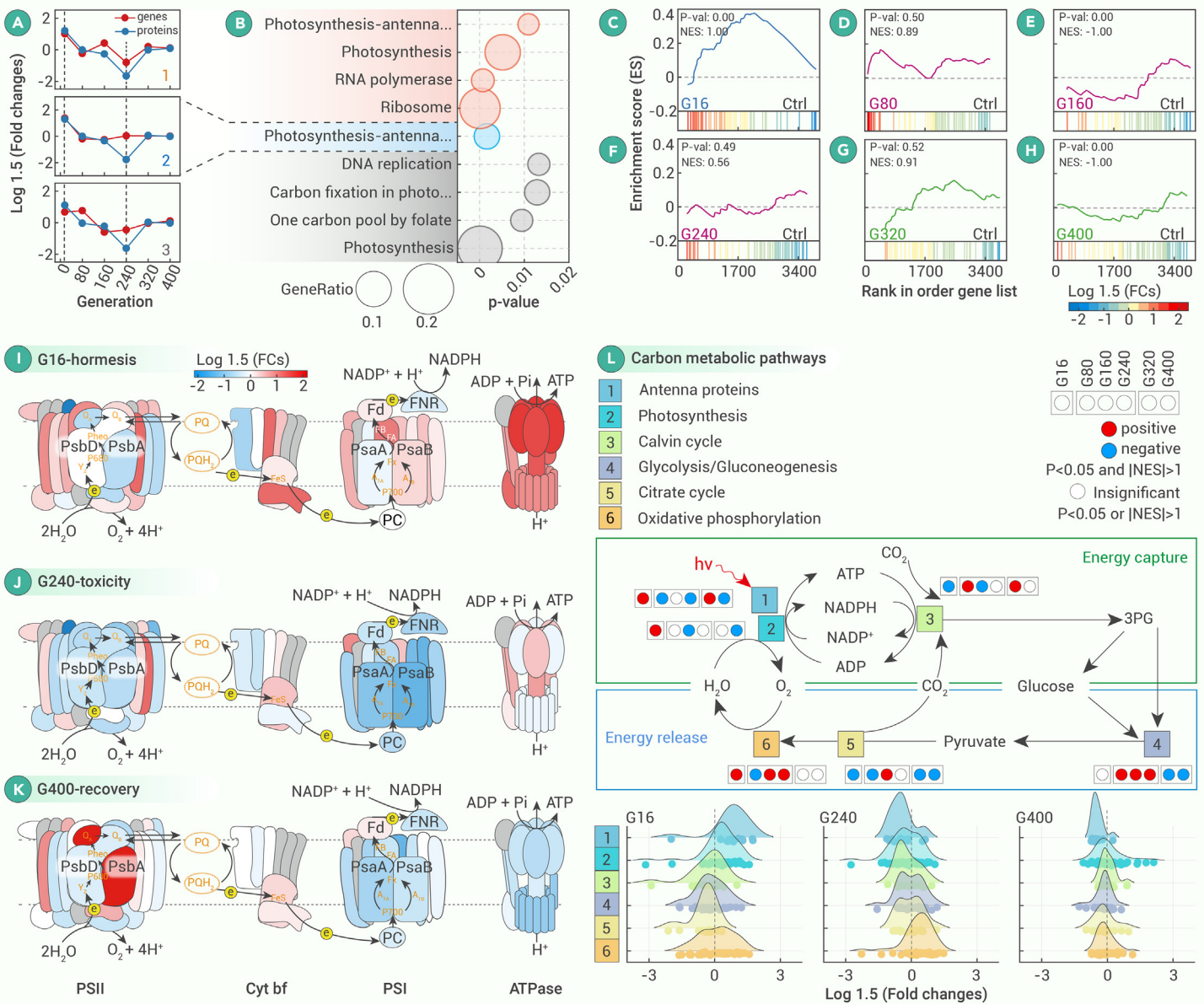
Figure 4. Gene and protein expression signatures during 6PPD-Q exposure (A) Clustering of genes in *Synechocystis* sp. exposed to 6PPD-Q for 16, 80, 160, 240, 320, and 400 generations (G16, G80, G160, G240, G320, and G400). Three clusters consistent with changes in cell density are shown here. (B) KEGG pathway enrichment of genes/proteins in each cluster. The gene ratio represents the proportion of genes mapped to KEGG pathways to the total number of genes in the pathway. (C–H) Gene set enrichment analysis (GSEA) enrichment of genes in the KEGG photosynthesis pathway (KEGG: syz00195) at G16, G80, G160, G240, G320, and G400. (I–K) Transcripts of photosynthetic electron transport chain (ETC)-associated genes (G16, G240, and G400) were selected to represent the hormesis, toxicity, and recovery phases, respectively. Genes involved in photosynthetic electron transfer are colored according to the fold changes in transcription. Gene names represented by each block and the results of G80 and G160 in the toxic phase and G320 in the recovery phase are given in Figure S9. (L) Central carbon metabolism of *Synechocystis* sp. exposed to 6PPD-Q for 400 generations. Top, study overview depicting central carbon metabolism, including energy capture (1, antenna proteins; 2, photosynthesis; and 3, Calvin cycle) and energy release (4, glycolysis/gluconeogenesis; 5, citrate cycle; and 6, oxidative phosphorylation) pathways, as well as the GSEA results for these pathways (Table S1). Bottom, ridgeline curves showing the fold change distribution of genes in 6 pathways. Each point represents a gene.

Additionally, 100 μg/L 6PPD-Q consistently inhibited carbon fixation in *Synechocystis* sp. over 400 generations. The carbon fixation rates decreased by approximately 6%, 30%, and 29% at G16, G240, and G400, respectively (Figures 6B–6D).

Additionally, the fate of 6PPD-Q in culture was also determined and is discussed in Text S4. The reduction in 6PPD-Q in the medium solutions predominantly resulted from cell metabolism (~40% and 21% for the 100 ng/L and 100 μg/L 6PPD-Q exposure groups, respectively), followed by hydrolysis and photodegradation (~36% and 33% for the 100 ng/L and 100 μg/L 6PPD-Q exposure groups, respectively). Intracellular accumulation did not significantly differ across generations, and the transfer of 6PPD-Q between exposure batches due to accumulation was minimal. Hence, the observed biological responses are primarily attributable to newly introduced 6PPD-Q in each exposure batch rather than carryover from previous exposures.

DISCUSSION

This study revealed the sequential responses of cyanobacteria to 6PPD-Q, including the hormesis, toxicity, and recovery phases, all of which occurred at environmentally relevant concentrations over 400 generations of exposure. To our knowledge, this is the first study documenting such long-term effects of environmental pollutants on cyanobacteria. Hormetic stimulation is increasingly common in cyanobacteria exposed to toxicants,[32,41] but few studies have tracked the long-term development of toxin-induced hormesis. In this study, *Synechocystis* sp. experienced adverse effects from 6PPD-Q for an extended period (~60 days) following short-term stimulation (~4 days). Although eventual recovery through self-adaptation was observed, the cumulative loss of biomass during this long-term exposure cannot be overlooked. These findings underscore the importance of considering the chronic and long-term effects of chemicals at
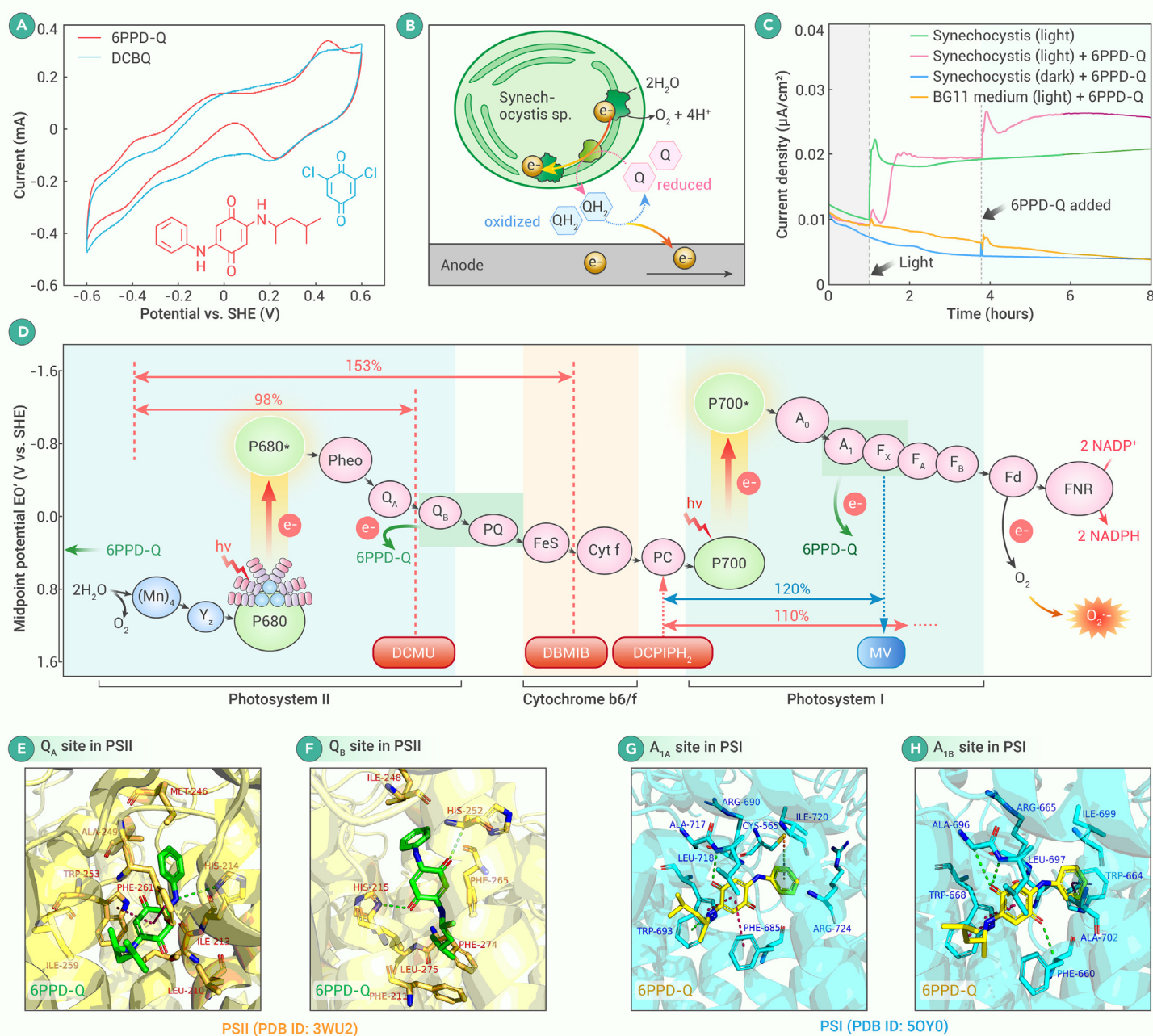
Figure 5. Evidence for 6PPD-Q accepting electrons from the photosynthetic ETC (A) Cyclic voltammograms of 6PPD-Q (red) and the typical exogenous electron acceptor 2,6-dichloro-1,4-benzoquinone (DCBQ) (blue). (B) Schematic illustration of a biophotovoltaic system employing cyanobacteria at the anode. In the indirect extracellular electron transfer pathway, 6PPD-Q mediates the electron transfer between the electrode surface and *Synechocystis* sp. 6PPD-Q in the oxidized form (Q) can be reduced (QH_2, the reduced form) after accepting electrons from the ETC. QH_2 is oxidized by the anode, producing currents and Q for new cycles. (C) Chronoamperograms of *Synechocystis* sp. with and without 6PPD-Q (1 mg/L). (D) The action sites of 6PPD-Q in the photosynthetic ETC. The target sites of 6PPD-Q in the ETC were measured by the oxygen evolution/consumption of *Synechocystis* sp. with photosynthesis inhibitors. The red dashed lines indicate the target sites of the inhibitors (3-(3,4-dichlorophenyl)-1,1-dimethylurea (DCMU) and 2,5-dibromo-3-methyl-6-isopropylbenzoquinone (DBMIB), which inhibit electron transfer from Q_A to the Q_B and from the plastoquinone (PQ) pool to the Rieske iron−sulfur (FeS) center, respectively. The target sites of the artificial electron donor reduced 2,6-dichlorophen-olindophenol ($DCPIPH_2$) and acceptor (methyl viologen [MV]) are indicated by red and blue dotted lines, respectively, with arrows. The results are expressed as the percentage of oxygen evolution/consumption in *Synechocystis* sp. treated with inhibitors with or without the addition of 6PPD-Q, and results greater than 100% indicate that 6PPD-Q was successfully photoreduced by photosynthetic electrons. Green shading highlights the electron-accepting sites of 6PPD-Q. (E−H) The docking positions of 6PPD-Q in the Q_A-binding pocket, Q_B-binding pocket, A_{1A}-binding pocket, and A_{1B}-binding pocket of PSII/PSI in *Synechocystis* sp. 6803. The docked ligands (i.e., 6PPD-Q) are depicted in green and yellow in PSII and PSI, respectively. The interacting residues are presented as yellow and cyan sticks in PSII and PSI, respectively. The interactions, including π-π stacking and hydrogen bonding, are represented by red and green dashed lines, respectively.

environmentally relevant concentrations, as the true toxicity of pollutants can be masked by minor variations or hormesis during a limited exposure period.

This study has elucidated the previously unknown toxicological mechanisms of 6PPD-Q in aquatic organisms. These findings provide strong evidence that 6PPD-Q disrupts photosynthesis by acting as an exogenous electron acceptor and interfering with photosynthetic electron transport. During the initial exposure to 6PPD-Q, *Synechocystis* sp. increased photosynthetic electron production as a defense strategy against electron extraction but reduced Rubisco activity in the CBB cycle, creating a hormetic trade-off. This leads to an energy source-sink imbalance, resulting in the accumulation of NADPH and ATP. To dissipate excess energy, *Synechocystis* sp. upregulated the following endogenous photoprotective pathways: electron flux to flavodiiron proteins[42] and respiratory terminal oxidases[43] (Figure S14). Simultaneously, they reduced light absorption, downregulated PSII and PSI activity, and inhibited linear electron flow, thereby correcting the energy source-sink imbalance (Figures 4 and S14). In this context, 6PPD-Q competes for electrons, reducing light energy utilization for cell growth and exhibiting toxic effects on *Synechocystis* sp. (G16−G240). Surprisingly, the activity of Rubisco gradually increased during prolonged exposure to 6PPD-Q, expanding
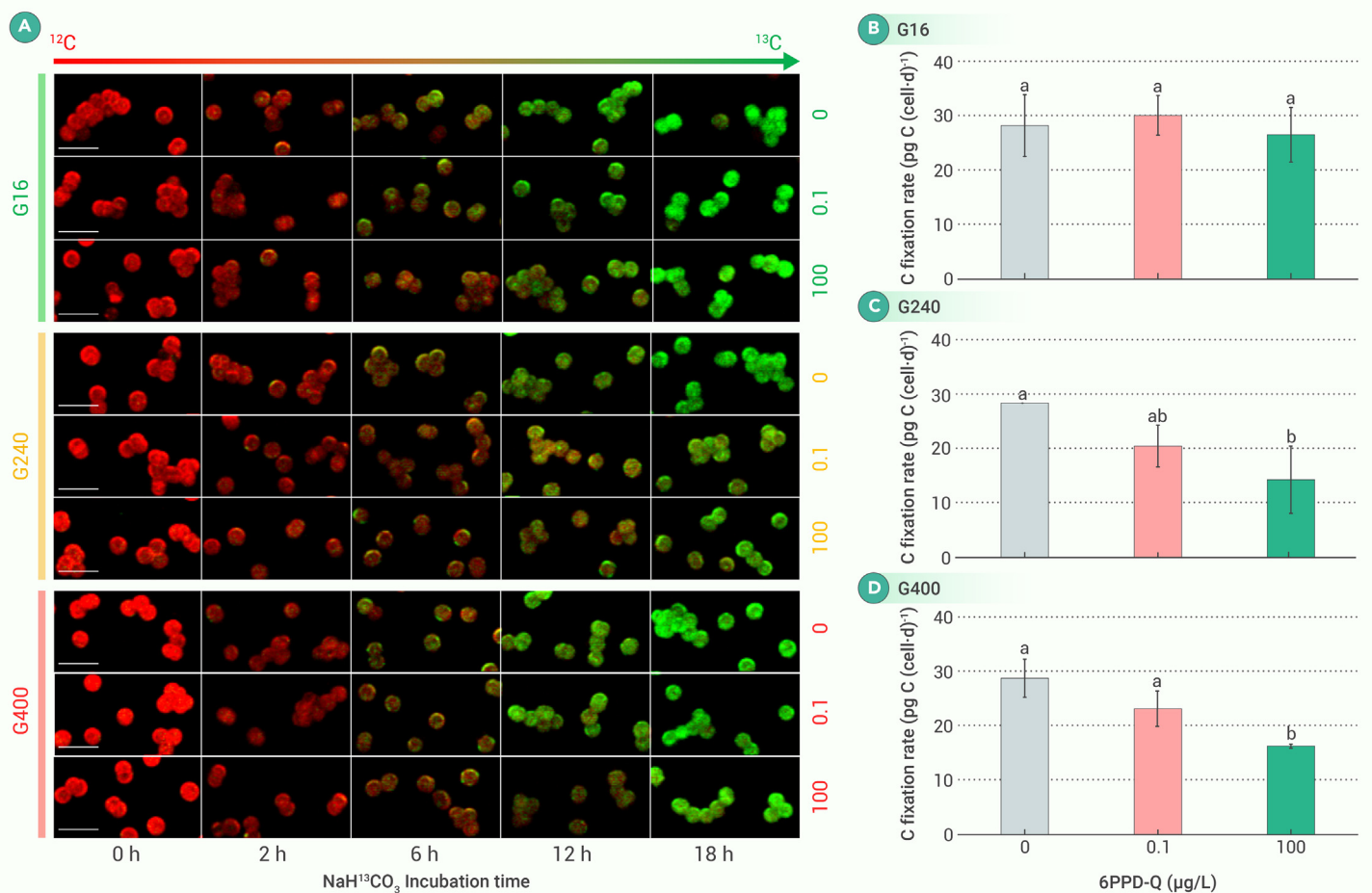
Figure 6. Carbon fixation rates of *Synechocystis* sp. (A) Raman images of cells incubated with ^{13}C-NaHCO$_3$ for 18 h under light conditions. Scale bars, 6 μm. (B–D) Carbon fixation rates of *Synechocystis* sp. with a 14:10 h light-dark cycle detected by isotope mass spectrometry (significant differences in carbon fixation rates among different treatments are marked with different letters; one-way ANOVA).

the sinks for CO_2 assimilation (Figures S6 and S14). This improvement in CO_2 assimilation ability enabled the recovery of previously inhibited cell growth, eventually reaching a level comparable to that of the control (G240–G400). Ultimately, the cells establish new energy homeostasis by continuously regulating the balance between sources and sinks. This adaptive response allows them to cope with prolonged exposure to 6PPD-Q and maintain their growth (Figure S14).

CO_2 is the ultimate electron acceptor for photochemically generated electrons in the process of photosynthesis.[37] 6PPD-Q intercepts photoelectrons from the photosynthetic ETC, inducing a decrease in CO_2 assimilation. The carbon fixation rate showed a sustained reduction at G240 and G400 following an initial increase at G16 upon exposure to 0.1 μg/L 6PPD-Q (Figures 6B–6D). This reduction in biomass and carbon fixation rates highlights the significant impact of 6PPD-Q on primary production in aquatic environments.

In addition to influencing photosynthesis, 6PPD-Q may also regulate CO_2 assimilation in cyanobacteria through its potential impact on the respiratory ETC. Despite the involvement of the PQ pool in both the photosynthetic and respiratory ETCs, the observed changes in CO_2 assimilation upon 6PPD-Q exposure were primarily attributed to photosynthetic dysregulation. However, the contribution of respiration regulation cannot be excluded. Further investigation is required to determine whether 6PPD-Q disturbs respiratory electron transfer and contributes to the observed changes in carbon fixation.

Quinone-type compounds, including synthetic quinones such as 6PPD-Q, can disrupt the flow of photoelectrons to the organic carbon sink, thereby impacting the carbon fixation of primary producers. This common feature of quinones suggests that they can disturb the photosynthetic carbon fixation process in cyanobacteria. These findings enhance our understanding of the toxic effects of quinone pollutants on cyanobacteria and provide a valuable framework for studying the effects of quinone compounds on photosynthetic carbon fixation in cyanobacteria.

MATERIALS AND METHODS

See the supplemental information for details.

REFERENCES

1. Guzman, M.S., Rengasamy, K., Binkley, M.M., et al. (2019). Phototrophic extracellular electron uptake is linked to carbon dioxide fixation in the bacterium *Rhodopseudomonas palustris*. Nat. Commun. **10**(1): 1355. https://doi.org/10.1038/s41467-019-09377-6.
2. Wang, Y., Xu, W., Yuan, W., et al. (2021). Higher plant photosynthetic capability in autumn responding to low atmospheric vapor pressure deficit. Innovation **2**(4): 100163. https://doi.org/10.1016/j.xinn.2021.100163.
3. Tan, C., Xu, P., and Tao, F. (2022). Carbon-negative synthetic biology: challenges and emerging trends of cyanobacterial technology. Trends Biotechnol. **40**(12): 1488–1502. https://doi.org/10.1016/j.tibtech.2022.09.012.
4. Waterbury, J.B., Watson, S.W., Guillard, R.R., et al. (1979). Widespread occurrence of a unicellular, marine, planktonic, cyanobacterium. Nature **277**(5694): 293–294. https://doi.org/10.1038/277293a0.
5. Pisciotta, J.M., Zou, Y., and Baskakov, I.V. (2010). Light-dependent electrogenic activity of cyanobacteria. PLoS One **5**(5): e10821. https://doi.org/10.1371/journal.pone.0010821.
6. Ji, X., Verspagen, J.M.H., Van de Waal, D.B., et al. (2020). Phenotypic plasticity of carbon fixation stimulates cyanobacterial blooms at elevated CO_2. Sci. Adv. **6**(8): eaax2926. https://doi.org/10.1126/sciadv.aax292.
7. Ostrach, D.J., Low-Marchelli, J.M., Eder, K.J., et al. (2008). Maternal transfer of xenobiotics and effects on larval striped bass in the San Francisco Estuary. Proc. Natl. Acad. Sci. USA **105**(49): 19354–19359.
8. Li, S., Liu, Y., Wu, Y., et al. (2022). Antibiotics in global rivers. Natl. Sci. Open **1**(2): 20220029. https://doi.org/10.1360/nso/20220029.
9. Ramakrishnan, B., Megharaj, M., Venkateswarlu, K., et al. (2010). The impacts of environmental pollutants on microalgae and cyanobacteria. Crit. Rev. Env. Sci. Tec. **40**(8): 699–821. https://doi.org/10.1080/10643380802471068.
10. You, X., Li, H., Pan, B., et al. (2022). Interactions between antibiotics and heavy metals determine their combined toxicity to *Synechocystis* sp. J. Hazard Mater. **424**: 127707. https://doi.org/10.1080/10643380802471068.

11. You, X., You, M., Lyu, Y., et al. (2022). Single and combined exposure to micro (nano) plastics and azithromycin disturbing the photosynthetic carbon fixation of *Synechocystis* sp. Environ. Sci. Nano **9**(12): 4354–4366. https://doi.org/10.1039/D2EN00204C.

12. Monks, T.J., and Jones, D.C. (2002). The metabolism and toxicity of quinones, quinonimines, quinone methides, and quinone-thioethers. Curr. Drug Metab. **3**(4): 425–438. https://doi.org/10.2174/1389200023337388.

13. Ve Van, L., Tran, Q.G., Ko, S.R., et al. (2022). How do freshwater microalgae and cyanobacteria respond to antibiotics? Crit. Rev. Biotechnol. **43**(2): 191–211. https://doi.org/10.1080/07388551.2022.2026870.

14. Chen, F., Xiao, Z., Yue, L., et al. (2019). Algae response to engineered nanoparticles: current understanding, mechanisms and implications. Environ. Sci.: Nano **6**(4): 1026–1042. https://doi.org/10.1039/c8en01368c.

15. Amaneesh, C., Anna Balan, S., Silpa, P.S., et al. (2023). Gross negligence: impacts of microplastics and plastic leachates on phytoplankton community and ecosystem dynamics. Environ. Sci. Technol. **57**(1): 5–24. https://doi.org/10.1021/acs.est.2c05817.

16. Gu, J., Song, Y., Yang, Y., et al. (2022). Mechanical insights into activation of peroxides by quinones: Formation of oxygen-centered radicals or singlet oxygen. Environ. Sci. Technol. **56**(12): 8776–8783. https://doi.org/10.1021/acs.est.1c08883.

17. Jakober, C.A., Riddle, S.G., Robert, M.A., et al. (2007). Quinone emissions from gasoline and diesel motor vehicles. Environ. Sci. Technol. **41**(13): 4548–4554. https://doi.org/10.1021/es062967u.

18. Lotina-Hennsen, B., Achnine, L., Ruvalcaba, N.M., et al. (1998). 2,5-diamino-p-benzoquinone derivatives as photosystem I electron acceptors: Synthesis and electrochemical and physicochemical properties. J. Agric. Food Chem. **46**(2): 724–730. https://doi.org/10.1021/jf970979g.

19. Fu, H.Y., Picot, D., Choquet, Y., et al. (2017). Redesigning the Q(A) binding site of Photosystem II allows reduction of exogenous quinones. Nat. Commun. **8**(1): 15274. https://doi.org/10.1038/ncomms15274.

20. Longatte, G., Rappaport, F., Wollman, F.A., et al. (2016). Mechanism and analyses for extracting photosynthetic electrons using exogenous quinones - what makes a good extraction pathway? Photochem. Photobiol. Sci. **15**(8): 969–979. https://doi.org/10.1039/c6pp00076b.

21. Tian, Z., Zhao, H., Peter, K.T., et al. (2021). A ubiquitous tire rubber–derived chemical induces acute mortality in coho salmon. Science **371**(6525): 185–189. https://doi.org/10.1126/science.abd6951.

22. Hiki, K., Asahina, K., Kato, K., et al. (2021). Acute toxicity of a tire rubber-derived chemical, 6PPD quinone, to freshwater fish and crustacean species. Environ. Sci. Technol. Lett. **8**(9): 779–784. https://doi.org/10.1021/acs.estlett.1c00453.

23. Challis, J.K., Popick, H., Prajapati, S., et al. (2021). Occurrences of tire rubber-derived contaminants in cold-climate urban runoff. Environ. Sci. Technol. Lett. **8**(11): 961–967. https://doi.org/10.1021/acs.estlett.1c00682.

24. Johannessen, C., Helm, P., and Metcalfe, C.D. (2021). Detection of selected tire wear compounds in urban receiving waters. Environ. Pollut. **287**: 117659. https://doi.org/10.1016/j.envpol.2021.117659.

25. Johannessen, C., Helm, P., Lashuk, B., et al. (2022). The tire wear compounds 6PPD-quinone and 1, 3-diphenylguanidine in an urban watershed. Arch. Environ. Con. Tox. **82**(2): 171–179. https://doi.org/10.1007/s00244-021-00878-4.

26. Rauert, C., Charlton, N., Okoffo, E.D., et al. (2022). Concentrations of tire additive chemicals and tire road wear particles in an australian urban tributary. Environ. Sci. Technol. **56**(4): 2421–2431. https://doi.org/10.1021/acs.est.1c07451.

27. French, B.F., Baldwin, D.H., Cameron, J., et al. (2022). Urban roadway runoff is lethal to juvenile coho, steelhead, and Chinook salmonids, but not congeneric sockeye. Environ. Sci. Technol. Lett. **9**(9): 733–738. https://doi.org/10.1021/acs.estlett.2c00467.

28. Brinkmann, M., Montgomery, D., Selinger, S., et al. (2022). Acute toxicity of the tire rubber-derived chemical 6PPD-quinone to four fishes of commercial, cultural, and ecological importance. Environ. Sci. Technol. Lett. **9**(4): 333–338. https://doi.org/10.1021/acs.estlett.2c00050.

29. Zhang, Y., Calabrese, E.J., Zhang, J., et al. (2020). A trigger mechanism of herbicides to phytoplankton blooms: From the standpoint of hormesis involving cytochrome b559, reactive oxygen species and nitric oxide. Water Res. **173**: 115584. https://doi.org/10.1016/j.watres.2020.115584.

30. Calabrese, E.J. (2013). Hormetic mechanisms. Crit. Rev. Toxicol. **43**(7): 580–606. https://doi.org/10.3109/10408444.2013.808172.

31. Moustakas, M., Moustaka, J., and Sperdouli, I. (2022). Hormesis in photosystem II: a mechanistic understanding. Curr. Opin. Toxicol. **29**: 57–64. https://doi.org/10.1016/j.cotox.2022.02.003.

32. Erofeeva, E.A. (2022). Environmental hormesis of non-specific and specific adaptive mechanisms in plants. Sci. Total Environ. **804**: 150059. https://doi.org/10.1016/j.scitotenv.2021.150059.

33. Jager, T., Barsi, A., and Ducrot, V. (2013). Hormesis on life-history traits: is there such thing as a free lunch? Ecotoxicology **22**(2): 263–270. https://doi.org/10.1007/s10646-012-1022-0.

34. Liberton, M., Page, L.E., O'Dell, W.B., et al. (2013). Organization and flexibility of cyanobacterial thylakoid membranes examined by neutron scattering. J. Biol. Chem. **288**(5): 3632–3640. https://doi.org/10.1074/jbc.M112.416933.

35. Liberton, M., Collins, A.M., Page, L.E., et al. (2013). Probing the consequences of antenna modification in cyanobacteria. Photosynth. Res. **118**: 17–24. https://doi.org/10.1007/s11120-013-9940-0.

36. Van Eerden, F.J., Melo, M.N., Frederix, P.W., et al. (2017). Exchange pathways of plastoquinone and plastoquinol in the photosystem II complex. Nat. Commun. **8**(1): 15214–15218. https://doi.org/10.1038/ncomms15214.

37. Santos-Merino, M., Torrado, A., Davis, G.A., et al. (2021). Improved photosynthetic capacity and photosystem I oxidation via heterologous metabolism engineering in cyanobacteria. Proc. Natl. Acad. Sci. USA **118**(11): e2021523118. https://doi.org/10.1073/pnas.2021523118.

38. Nikkanen, L., Solymosi, D., Jokel, M., et al. (2021). Regulatory electron transport pathways of photosynthesis in cyanobacteria and microalgae: Recent advances and biotechnological prospects. Physiol. Plant. **173**(2): 514–525. https://doi.org/10.1111/ppl.13404.

39. Hauser, T., Popilka, L., Hartl, F.U., et al. (2015). Role of auxiliary proteins in Rubisco biogenesis and function. Nat. Plants **1**(6): 1–11. https://doi.org/10.1038/nplants.2015.65.

40. Cardol, P., Forti, G., and Finazzi, G. (2011). Regulation of electron transport in microalgae. Biochim. Biophys. Acta **1807**(8): 912–918. https://doi.org/10.1016/j.bbabio.2010.12.004.

41. Agathokleous, E., Guo, J., Peñuelas, J.J.R., et al. (2022). Low doses of toxicants can enhance algae potential as biodiesel and biomass feedstocks. Renew. Sustain. Energy Rev. **168**: 112858. https://doi.org/10.1016/j.rser.2022.112858.

42. Allahverdiyeva, Y., Mustila, H., Ermakova, M., et al. (2013). Flavodiiron proteins Flv1 and Flv3 enable cyanobacterial growth and photosynthesis under fluctuating light. Proc. Natl. Acad. Sci. USA **110**(10): 4111–4116. https://doi.org/10.1073/pnas.1221194110.

43. Ermakova, M., Huokko, T., Richaud, P., et al. (2016). Distinguishing the roles of thylakoid respiratory terminal oxidases in the cyanobacterium *Synechocystis* sp. PCC 6803. Plant Physiol. **171**(2): 1307–1319. https://doi.org/10.1104/pp.16.00479.

AUTHOR CONTRIBUTIONS

X.Y. and W.S. conceived the idea and designed the research. X.Y. and X.C performed the experiment. Y.J., H.C., J.L., Z.W., and J.N. provided constructive suggestions for the results and discussion. X.Y. and W.S. contributed to writing the manuscript. W.S. supervised the project.

DECLARATION OF INTERESTS

The authors declare no competing interests.

SUPPLEMENTAL INFORMATION

It can be found online at https://doi.org/10.1016/j.xinn.2024.100630.

LEAD CONTACT WEBSITE

http://scholar.pku.edu.cn/swl